SPECIAL PUBLICATION OF THE GEOLOGICAL SOCIETY OF INDIA
No.13, 2026, pp. 113–124

Vibrational Spectroscopic Studies of Selected Critical Minerals from India using FTIR and Laser Micro-Raman Methods

Bhaskar J. Saikia[1]*, G. Parthasarathy[2,3#], Rashmi R. Borah[4], and B. Saravanan[5]

[1]Department of Physics, Anandaram Dhekial Phookan College, Nagaon - 782002, India
[2]School of Natural and Engineering Sciences, National Institute of Advanced Studies, IISc, Bengaluru - 560012, India
[3]Raja Ramanna Chair Professor, Atomic Minerals Directorate for Exploration & Research (AMD), Department of Atomic Energy, Naagarabhaavi, Bengaluru - 560072, India
[4]Department of Physics, Nagaon University, Nagaon - 782001, India
[5]Atomic Minerals Directorate for Exploration and Research, Begumpet, Hyderabad - 500016, India
***E-mail:** vaskaradp@gmail.com,*
***#E-mail**: partha@nias.res.in, partha.dae.amd@gmail.com*
Received 27 June 2026; Revised 05 August 2026; Accepted 20 August 2026

Abstract: Critical minerals are essential for modern technologies, renewable energy systems, and national strategic priorities. This review presents spectroscopic data on selected critical minerals from India, including lithium-, titanium-, tungsten-, vanadium-, and tin-bearing minerals, as well as fluid-deposited graphite. The study highlights the capabilities of Fourier transform infrared (FTIR) and laser micro-Raman spectroscopy as rapid, non-destructive, and cost-effective approaches for mineral characterization. Particular emphasis is placed on the limitations of conventional analytical techniques such as X-ray fluorescence (XRF) and electron probe microanalysis (EPMA) for characterizing lithium-bearing minerals. These limitations mainly arise from the low atomic number of lithium and its occurrence at low concentrations, which hinder its reliable detection and quantification by conventional analytical techniques.

The minerals discussed in this review are based on our experimental investigations and include fluid-deposited natural graphite, the lithium-bearing mineral cookeite from Jammu, tungsten-bearing minerals, nanocrystalline cassiterite from the Eastern Ghats—the principal economic ore of tin—Schreyerite ($V_2Ti_3O_9$), a rare vanadium–titanium oxide mineral from the Pb–Zn ore deposit of Bhilwara, Rajasthan, vanadium-bearing cavansite from the Deccan Traps, and geikielite from Southern Granulite Terrain, Tamil Nadu.

The results demonstrate that Raman and FTIR spectroscopy provide valuable information on molecular structure, bonding environments, crystallinity, mineral identification, and phase characteristics, while complementing conventional analytical techniques. This review highlights the potential of vibrational spectroscopic methods for the identification, characterization, mapping, and processing of strategic mineral resources. Although this review focuses on selected critical minerals, including lithium-, titanium-, vanadium-, tin-, and tungsten-bearing minerals, the approaches discussed are applicable to other critical mineral systems, such as cobalt-, nickel-, and rare earth element (REE)-bearing minerals. This review provides a framework for applying vibrational spectroscopy to the exploration, characterization, and sustainable development of India's critical mineral resources.

Keywords: Natural Resources; Critical Minerals; Raman; Infrared; Spectroscopic Methods.

INTRODUCTION

The application of Raman and infrared spectroscopy provides a powerful framework for the characterization of critical minerals, offering valuable insights into crystal chemistry, mineral stability, and ore-forming processes through rapid and non-destructive analysis. (Frost, 1995; Frost and Rintoul, 1996; Nayak and Singh, 2007; Jehlička and Edwards, 2008; Ritz et al., 2012; Pani et al., 2016; Kumar and Lingfa, 2020). These vibrational spectroscopic techniques provide rapid and reliable identification of economically important mineral phases, including lithium-bearing silicates and phyllosilicates, titanium-bearing refractory

Recommended Citation:
Saikia, B.J., Parthasarathy, G., Borah, R.R. and Saravanan, B. (2026). Vibrational Spectroscopic Studies of Selected Critical Minerals from India using FTIR and Laser Micro-Raman Methods. In: *Natural Resources and their Utilisation with Special Reference to Critical Minerals* (Ed.: Mohanty, S.P.). Special Publication of the Geological Society of India (Bengaluru), 13, id:174488. https://doi.org/10.17491/CGSI.2026.174488

oxides, and hydrous framework silicates. Raman spectroscopy is particularly effective in distinguishing mineral polymorphs, determining cation coordination, evaluating crystallinity, and detecting nanoscale intergrowths, while infrared spectroscopy offers complementary information on hydroxyl groups, water content, hydrogen-bonding environments, and structural disorder (Saikia et al., 2008). Together, they enable detailed characterization of mineral assemblages, alteration products, and phase relationships that are often difficult to resolve using conventional methods alone.

As the global demand for critical minerals continues to increase because of their importance in clean-energy technologies, advanced electronics, catalysis, aerospace applications, and energy storage systems, Raman and infrared spectroscopy play an increasingly important role in mineral exploration, resource evaluation, beneficiation studies, and environmental monitoring (Kelemen and Fang, 2001; Pani et al., 2016; Schito et al., 2017; Henry et al., 2019; Moroz et al., 2021; Harmon, 2024; Peng et al., 2026). The integration of these spectroscopic methods with complementary mineralogical, geochemical, and high-pressure techniques offers a robust framework for understanding the origin, evolution, and technological significance of critical mineral resources, thereby supporting sustainable exploration and utilization strategies (Zhou and Zihyun, 2025).

This review article summarizes our Raman and Fourier Transform Infrared (FTIR) spectroscopic investigations of selected critical minerals from India. The studies encompass the identification and characterization of lithium-bearing minerals, including cookeite and spodumene; titanium-bearing refractory minerals such as schreyerite ($V_2Ti_3O_9$); tungsten- and tin-bearing minerals; fluid-deposited graphite; and the investigation of pressure-induced structural transformations in hydrous silicates such as cavansite.

Beyond mineral identification, Raman and FTIR spectroscopy provide valuable insights into crystallization processes, hydrothermal alteration, fluid–rock interactions, cation distribution, and phase-transition mechanisms (Rull-Pérez and Martinez-Frias, 2006; Courrèges-Lacoste et al., 2007; Nayak and Singh, 2007; Jehlička and Edwards, 2008). These vibrational spectroscopic techniques are particularly effective in characterizing minerals that are difficult to investigate using conventional methods such as X-ray Fluorescence (XRF) and Electron Probe Microanalysis (EPMA), especially in the case of lithium-bearing phases where the low atomic number of lithium and the trace occurrence of the minerals pose significant analytical challenges (Saikia et al., 2026).

This review demonstrates the broad applicability of vibrational spectroscopy in the characterization of selected critical minerals and highlights its significance for mineral exploration, resource assessment, and sustainable resource development. Raman and FTIR spectroscopy provide rapid, non-destructive, and cost-effective approaches for characterization of mineral phases, crystal structures, lattice dynamics, chemical substitutions, and defect chemistry (Pani et al., 2016). When integrated with complementary analytical techniques such as electron microscopy, X-ray diffraction, electron probe microanalysis, and isotopic analyses, vibrational spectroscopy enables a comprehensive understanding of the mineralogy, geochemistry, and evolution of critical mineral deposits. Furthermore, its capability to investigate minerals under both ambient and high-pressure conditions extends its applications to deep-Earth processes and planetary materials. With the growing global demand for critical raw materials, vibrational spectroscopy is expected to play an increasingly important role in the discovery, characterization, and sustainable utilization of strategic mineral resources, including lithium, titanium, vanadium, tin, tungsten, cobalt, nickel, and rare earth elements (REEs). To our knowledge, this is one of the few reviews focusing specifically on FTIR and Raman spectroscopic investigations of selected critical minerals from India.

MATERIALS AND METHODS

The samples studied here are the naturally occurring minerals collected from diverse geological environments across India. Nanocrystalline cookeite was collected from the lithium-bearing pegmatites of the Reasi district, Jammu and Kashmir (Saikia et al., 2026). Cavansite and associated zeolite minerals were obtained from the Deccan volcanic province at the Wagholi quarry, Pune, Maharashtra (Birch, 1977; Kothavala, 1991; Parthasarathy et al., 2008; Ravindran et al., 2012). Fluid-deposited graphite samples were collected from the Achan-Kovil Shear Zone and the Burugubanda–Tapasikonda graphite–tungsten deposits of the Eastern Ghats Mobile Belt (EGMB), Andhra Pradesh, India (Biswal et al., 2000; Parthasarathy et al., 2006a,b). The Burugubanda–Tapasikonda deposits were formed during widespread tectonothermal events associated with the evolution of the EGMB and comprise rare epigenetic, rhombohedral graphite precipitated from carbon-bearing hydrothermal fluids. These graphite deposits are closely associated with granodioritic intrusions, fluid–rock interactions, and tungsten mineralization, and represent one of only four known occurrences of fluid-deposited rhombohedral graphite worldwide, the others being reported from Sri Lanka, Spain, and England (Ramakrishnan et al., 1998; Parthasarathy et al., 2006a,b; Umathay and Pophare, 2014). Thus, they constitute an important natural analogue for investigating hydrothermal carbon precipitation and graphite-associated ore-forming processes. Natural cassiterite samples were collected from the Bastar Craton, Chhattisgarh, particularly the Dantewada and Sukma districts, where tin mineralization is associated with Proterozoic granites and pegmatites (Acharya et al., 1982; Babu, 1994; Parthasarathy and Sreedhar, 2011). Cassiterite commonly occurs as well-formed tetragonal crystals, massive aggregates, and detrital grains in alluvial placer deposits, and is typically associated with quartz, topaz, tourmaline, wolframite, columbite–tantalite, fluorite, muscovite, and other granitic minerals. Trace elements such as Fe, Nb, Ta, W, Ti, and Mn are commonly incorporated into the cassiterite lattice and provide valuable information on the origin, evolution, and physicochemical conditions of tin-bearing hydrothermal systems. Naturally occurring geikielite crystals (1–4 mm in size) were collected from a calc-silicate marble quarry in the ~550 Ma Southern Granulite Terrain near Rajapalayam, Tamil Nadu, India (Janardhan et al., 2001; Chandra et al., 2010). The geological setting and petrogenesis of the geikielite-bearing assemblage have been described in detail elsewhere (Janardhan et al., 2001).

The experimental procedures and vibrational spectroscopic techniques employed in this study have been described in detail in our previous publications (Saikia et al., 2008, 2009, 2010, 2016, 2017,

2018, 2021, 2022a,b,c,d, 2023, 2024, 2026). Raman spectroscopic measurements were performed on bulk powdered samples using a Jobin-Yvon Horiba LabRAM HR micro-Raman spectrometer (Horiba Scientific, USA) coupled to an Olympus optical microscope equipped with 10×, 50×, and 100× objectives, providing a laser spot size of ~0.5–2 µm. Excitation was provided by 514, 532, and 632.8 nm laser sources with an incident power of ~5 mW, selected according to the optical characteristics of each mineral to minimize fluorescence and thermal effects (e.g., cassiterite: 532 and 632.8 nm; schreyerite: 514 and 532 nm; scheelite: 532 and 632.8 nm; cavansite: 532 and 632.8 nm; graphite: 514 and 532 nm). Spectra were collected over the 100–3000 cm^{-1} spectral range using an 1800 grooves mm^{-1} diffraction grating and a motorized x–y stage. Instrument calibration was performed using the first-order Raman band of a silicon wafer at 520.7 ± 0.5 cm^{-1}, yielding a spectral accuracy of ±0.5 cm^{-1} and a precision of ±0.1 cm^{-1}. An edge filter was employed to isolate the Stokes Raman scattering. Spectra were acquired at room temperature (≈28-30 °C) with integration times ranging from 10 to 60 s, depending on the Raman scattering efficiency and sample fluorescence. The acquired spectra were processed by baseline correction and Gaussian peak fitting to determine band positions accurately. Mineral identification was achieved by comparing the observed Raman spectra with reference spectra available in the RRUFF mineral database.

The infrared spectra were acquired using Perkin-Elmer Spectrum 2000 FTIR spectrophotometer (Model no. Spectrum Two, Make: PerkinElmer) with helium-neon laser as the source reference, at a resolution of 4cm^{-1}. A small agate mortar was used to properly grind and combine the sample with KBr in a ratio of 1:20 mixture before creating the sample pellet. The spectra were taken in transmission mode in the region 400 - 4000 cm^{-1}. The room temperature was 28°C during the experiment. The absorption bands of the functional groups are evaluated by using the software associated with the system.

RESULTS AND DISCUSSIONS

Graphite

Raman spectroscopy has become a widely used and reliable technique for investigating the crystallinity, structural order, and metamorphic evolution of carbonaceous materials in geological environments. Studies of graphite from the Burugubanda–Tapasikonda shear zone in the Proterozoic Eastern Ghats Mobile Belt (EGB), India, demonstrate the capability of Raman spectroscopy to distinguish fluid-deposited graphite from well-ordered crystalline graphite and to constrain metamorphic conditions (Dissanayake 1981; Wopenka and Pasteris, 1993; Luque et al., 1998; Ramakrishnan et al., 1998; Parthasarathy et al., 2006a,b). Combined X-ray diffraction and X-ray photoelectron spectroscopy revealed the coexistence of syngenetic hexagonal graphite and up to 20–25% epigenetic rhombohedral graphite, indicating precipitation from carbon-bearing fluids containing CO_2, CO, and CH_4 (Parthasarathy et al., 2006 a,b).

The Raman spectra are characterized by a prominent ordered (G or O) band (Fig.1) at 1581–1585 cm^{-1}, corresponding to the E_{2g} vibration of graphitic carbon, and a disorder-induced (D) band at 1351–1355 cm^{-1} associated with structural defects and heteroatom incorporation (Saikia et al., 2017, 2018, 2022d, 2023). The intensity ratio of the disorder to ordered bands (D/O ≈ 0.09–0.10) indicates a high degree of graphitization and is consistent with graphite formed

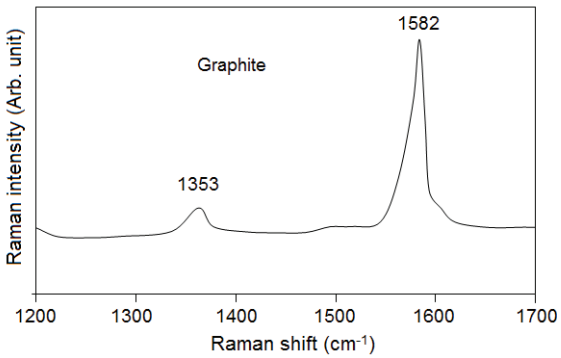


Fig. 1. First-order Raman spectrum of fluid-deposited graphite from the Eastern Ghats Mobile Belt (EGB), showing the ordered (G) band at ~1582 cm^{-1} and the disorder-induced (D) band at ~1353 cm^{-1}. The D/G intensity ratio (~0.10) indicates well-crystallized graphite formed under sillimanite-grade metamorphic conditions.

under sillimanite-facies metamorphic conditions, corresponding to temperatures of approximately 750 ± 30°C (Sharma et al., 2000, 2001; Parthasarathy and Sharma, 2001; Parthasarathy et al., 2002, 2003). Raman-derived crystallite sizes (La ≈ 34 nm) further confirm the well-crystallized nature of the graphite and provide quantitative constraints on metamorphic grade.

The second-order Raman region (2500–3100 cm^{-1}) provides additional insights into graphite structure and genesis (Fig.2). Characteristic overtone and combination bands occur near 2450, 2725–2735, 2950, and 3248 cm^{-1}, reflecting advanced graphitization and three-dimensional structural ordering (Parthasarathy et al., 2006a,b; Saikia et al., 2009, 2018, 2023). The presence of a distinct band near 2946 cm^{-1}, attributed to C–H stretching vibrations, provides evidence for the involvement of carbon-bearing fluids during graphite formation. Furthermore, broadening of the principal graphite band relative to synthetic graphite suggests deformation or bending of graphite sheets associated with fluid deposition. These observations are consistent with the occurrence of high-density CO_2-rich fluids and ultrahigh-temperature metamorphism reported from the Eastern Ghats Mobile Belt (Beyssac et al., 2002; Sarkar et al., 2003).

Cookeite

Raman and FTIR spectroscopy have proven to be highly effective techniques for the identification and characterization of lithium-bearing phyllosilicates, particularly cookeite, and their relationships with associated aluminosilicate minerals such as kaolinite and spodumene. Raman spectroscopy is especially valuable because it is sensitive to crystal structure, cation coordination, and lattice dynamics, enabling the recognition of fine-grained and nanocrystalline Li-bearing phases that may be difficult to identify using conventional methods. Our recent investigations of nano-crystalline cookeite inclusions in spodumene have established a set of characteristic Raman bands that serve as diagnostic fingerprints for this Li-rich chlorite-group mineral (Saikia et al., 2026).

The Raman spectra of cookeite are dominated by vibrational features in the 100–1300 cm^{-1} region, corresponding to lattice modes, Al–O–Si bending vibrations, and Si–O stretching modes (Fig.3). In the low- to mid-wavenumber region (100–600 cm^{-1}),

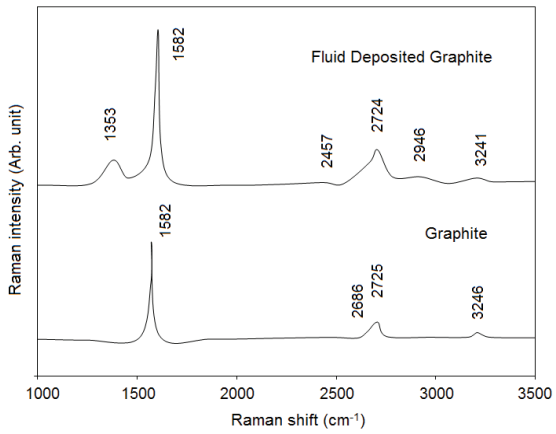


Fig. 2. Comparison of Raman spectra of fluid-deposited graphite from the Eastern Ghats Mobile Belt (EGB) and reference inorganic graphite, highlighting the first- and second-order Raman regions.

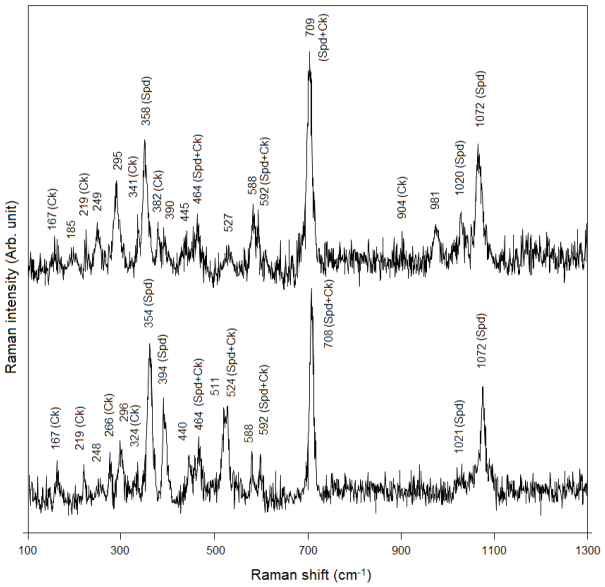


Fig. 3. Raman spectrum of Li-rich claystone from the Reasi area, Jammu, showing the characteristic vibrational bands of nanocrystalline cookeite and associated kaolinite in the 100–1300 cm^{-1} region (Spd: spodumene; Ck: cookeite).

characteristic Raman bands are observed at ~167, 219, 266, 341–342, 382, 464, and 592 cm^{-1}. The low-frequency bands (<300 cm^{-1}) are primarily attributed to lattice vibrations involving Li^{+} and Al^{3+} cations, whereas the higher-wavenumber bands (300–600 cm^{-1}) arise from bending vibrations of the LiO_6 and AlO_6 octahedra coupled with the SiO_4 tetrahedral framework (Li and Chou, 2016; Saikia et al., 2026). These observations are consistent with the work of Ding et al. (2020), who reported diagnostic cookeite bands at 98, 167, 219, 266, and 3640 cm^{-1} (Ding et al., 2020; Saikia et al., 2026). Bands near 266 and 324 cm^{-1} are assigned to tetrahedral–octahedral coupling and SiO_4 torsional vibrations associated with neighboring Li and Al sites, whereas bands near 382 and 464 cm^{-1} reflect Al–O–Si bending and chlorite-type sheet interactions. Peaks

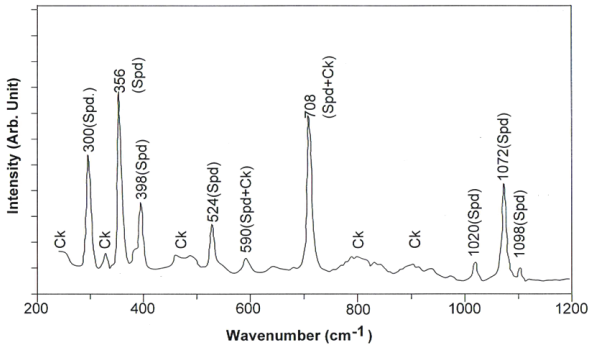


Fig. 4. Micro-Raman investigations of spodumene–cookeite assemblages in the range 200–1200 cm^{-1} provide further evidence for the coexistence of these phases and illustrate the capability of Raman spectroscopy to detect mineral intergrowths at the microscale.

near 527 and 588–592 cm^{-1} correspond to combined Si–O–Al bending and octahedral metal–oxygen stretching vibrations within the chlorite framework. In the higher-wavenumber region (900–1100 cm^{-1}), bands at 904, 1021–1027, and 1072 cm^{-1} are attributed to asymmetric Si–O stretching vibrations of isolated and bridging tetrahedra, although these features may overlap with signals from kaolinite and spodumene.

Micro-Raman investigations of spodumene–cookeite assemblages (Fig. 4) provide further evidence for the coexistence of these phases and illustrate the capability of Raman spectroscopy to detect mineral intergrowths at the microscale (Saikia et al., 2026). Composite spectra commonly arise when the laser beam simultaneously interacts with closely spaced or overlapping grains, producing combined spectral signatures of the constituent minerals (Saikia et al., 2017, 2022a, b, c, 2024). Diagnostic spodumene bands occur at 300, 356, 398, 524, 708, 1020, 1072, and 1098 cm^{-1} and correspond to lattice and Si–O stretching vibrations (Anderson et al., 2001; Pommier et al., 2003; Bobos et al., 2007; Anderson and Maccarron, 2011; Anderson, 2013; Saikia et al., 2026). Overlapping bands at approximately 266, 324, 382, 464, 524, 590, and 708 cm^{-1} indicate intimate intergrowths of cookeite and spodumene, while the broad nature of the cookeite bands relative to the sharper spodumene peaks reflects the nanocrystalline character of cookeite. Such textural and spectral relationships suggest that cookeite formed through hydrothermal alteration of primary spodumene, during which Li and Al were mobilized and subsequently reprecipitated under late-stage fluid-rich conditions (Anderson et al., 2001; Bobos et al., 2007; Anderson and Maccarron, 2011; Anderson, 2013; Saikia et al., 2026).

The infrared spectroscopy provides complementary information by probing framework vibrations and hydroxyl-bearing species, thereby enabling the characterization of kaolinite–cookeite assemblages and the evaluation of structural disorder (Fig. 5). In the mid-infrared region (400–1600 cm^{-1}), kaolinite exhibits strong absorption bands at 1140, 1084, 1066, and 1018 cm^{-1}, corresponding to Si–O stretching and Si–O–Al asymmetric stretching vibrations of tetrahedral silicate sheets (Farmer, 1974; Madejová and Komadel, 2001; Saikia and Parthasarathy, 2010; Saikia et al., 2016, 2021). The prominent band at 916 cm^{-1} is assigned to the Al–Al–OH

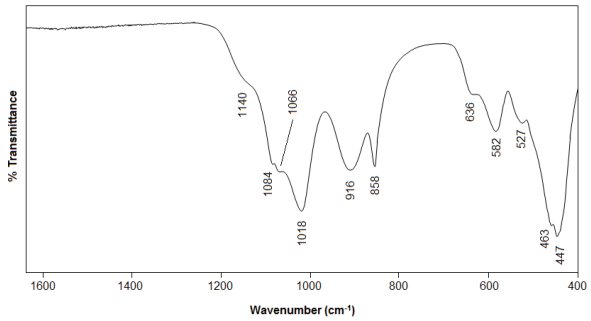


Fig. 5. Mid-infrared spectrum of Li-rich claystone from the Reasi area, Jammu, highlighting the characteristic vibrational bands of kaolinite and cookeite in the 400–1600 cm^{-1} region.

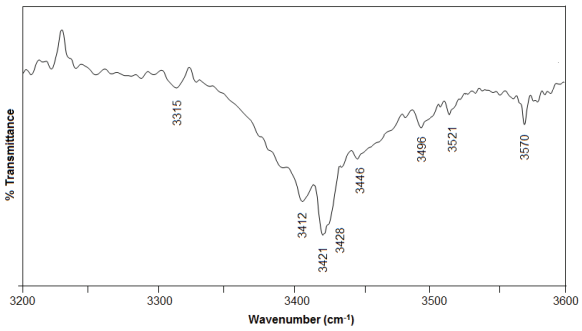


Fig. 6. Mid-infrared spectrum of Li-rich claystone from the Reasi area, Jammu, highlighting the OH-stretching vibrations of kaolinite and cookeite in the 3200–3600 cm^{-1} region.

deformation mode, whereas weaker absorptions near 858 cm^{-1} reflect Al–OH librational vibrations. Broad bands at 636 and 582 cm^{-1} arise from coupled Si–O–Al bending and metal–oxygen lattice vibrations, while features near 527 and 463–447 cm^{-1} are related to Al–O–Si deformation and octahedral metal–oxygen stretching modes. Although the FTIR spectra are dominated by kaolinite, broadened Si–O stretching bands in the 1084–1018 cm^{-1} region and enhanced absorption between 500 and 650 cm^{-1} reveal the presence of minor cookeite contributions (Saikia and Partasarathy, 2010; Saikia et al., 2026). In cookeite, Li–O and Al–O lattice vibrations occur primarily in the 500–650 cm^{-1} region, whereas broad Si–O–Al stretching modes appear between 1080 and 1010 cm^{-1}, reflecting the structural disorder typical of Li-bearing chlorite-group minerals. The resulting spectral overlap produces broadened composite features indicative of mixed-layer domains and nanocrystalline intergrowths.

The OH-stretching region of infrared spectrum (3200–3600 cm^{-1}) provides additional evidence for the coexistence of kaolinite and cookeite (Fig. 6). Well-ordered kaolinite is characterized by sharp OH-stretching bands near 3620, 3650, 3668, and 3695 cm^{-1}, corresponding to inner-surface and inner hydroxyl groups involved in hydrogen bonding (Farmer, 1974; Madejová and Komadel, 2001; Saikia and Parthasarathy, 2010). These FTIR bands complement Raman observations by providing direct information on hydroxyl environments, hydrogen bonding, and the degree of structural order, which are generally weak or absent in Raman spectra. While Raman spectroscopy is particularly sensitive to lattice vibrations associated with Si–O and Al–O frameworks, FTIR offers enhanced sensitivity to O–H stretching and bending vibrations. The combined use of Raman and FTIR spectroscopy therefore enables comprehensive characterization of kaolinite crystallinity, structural disorder, hydroxyl configuration, and mineral purity. In mixed kaolinite–cookeite assemblages, these absorptions become broadened and less resolved because of structural disorder and interlayer hydration. Broad bands between 3412 and 3446 cm^{-1} and a weaker shoulder near 3315 cm^{-1} are attributed to adsorbed or interlayer water and structurally bound hydroxyls associated with cookeite. Li–Al chlorites such as cookeite commonly display broad OH-stretching absorptions in the 3350–3470 cm^{-1} region, reflecting hydroxyl groups coordinated to Li^{+} and Al^{3+} cations (Wang et al., 2025; Saikia et al., 2026). Additional broad bands at 3532–3516 and 3355–3335 cm^{-1} provide strong evidence for Li–Al octahedral coordination within cookeite-rich domains (Wang et al., 2025; Saikia et al., 2026). These broad chlorite-related absorptions are superimposed on the sharper kaolinite OH bands, producing a composite spectral pattern characteristic of mixed-layer kaolinite–cookeite assemblages. Such spectral behavior is consistent with Raman observations and supports the interpretation that cookeite and kaolinite formed during late-stage hydrothermal alteration involving Li and Al mobilization, resulting in nanocrystalline intergrowths and complex phyllosilicate assemblages (Ding et al., 2020; Wang et al., 2025; Saikia et al., 2026). These techniques therefore play a critical role in understanding the mineralogy, crystal chemistry, and genesis of Li-bearing mineral systems and are increasingly important in the exploration and characterization of critical lithium resources.

Kaolinite is increasingly recognized as an important mineralogical host and geochemical indicator in the exploration of critical mineral resources, particularly ion-adsorption rare earth element (REE) deposits (Haxel et al., 2002; Moldoveanu and Papangelakis, 2012; Zhang et al., 2016; Xu et al., 2021). Its layered 1:1 aluminosilicate structure, high specific surface area, and negatively charged surfaces facilitate the adsorption and retention of trivalent REE ions from circulating groundwater and weathering fluids. As a result, kaolinite-rich weathering profiles can act as significant reservoirs for economically important REEs, including Nd and Dy. Unlike REEs hosted within primary mineral lattices, adsorbed REEs are weakly bound to clay surfaces and can be efficiently recovered through low-concentration acid leaching (Bradbury and Baeyens, 2002; Coppin et al., 2002; Moldoveanu and Papangelakis, 2013; Xiao et al., 2016; Alshameri et al., 2019). The vibrational spectroscopic techniques provide detailed information on crystal structure, hydroxyl environments, crystallinity, structural disorder, and fluid-induced alteration processes, thereby enabling the identification of kaolinite-rich horizons associated with REE mineralization. Furthermore, thermal pretreatment of kaolinite-bearing ores at temperatures around 600°C modifies the clay structure and enhances REE desorption and extraction efficiency, highlighting the importance of integrating clay mineralogy and vibrational spectroscopy in the exploration, beneficiation, and sustainable exploitation of critical mineral resources (Coppin et al., 2002; Saikia and Parthasarathy, 2010; Zhang et al., 2017).

Schreyerite

In addition, titanium-bearing refractory minerals such as schreyerite have received considerable attention because of their industrial and catalytic importance and their occurrence in planetary materials, including lunar samples and meteorites. The discovery of new Ti–V-bearing phases, such as machiite in the Murchison meteorite, further highlights the significance of these minerals in understanding planetary differentiation and high-temperature geological processes. Among these minerals, schreyerite ($V_2Ti_3O_9$) has been reported from metamorphic rocks in the Kwale District of Kenya, the Rampura–Agucha Zn–Pb–Ag deposit of Rajasthan, India, and the Lake Baikal region of Russia (Hoeller and Stumpfi, 1995; Dobelin et al., 2006). Detailed mineralogical investigations employing X-ray diffraction, thermal analysis, FTIR, and Raman spectroscopy have confirmed the monoclinic structure and high thermal stability of schreyerite (Parthasarathy et al., 2017). Raman spectroscopy is particularly important for the characterization of this mineral because it provides direct information on the local coordination environment of Ti and V through diagnostic vibrational modes. The prominent Raman bands near 438 cm^{-1} and 968 cm^{-1} are attributed to Ti–O and V=O vibrations, respectively, while the band at ~1040 cm^{-1} indicates tetrahedrally coordinated vanadium. These spectral fingerprints enable rapid and non-destructive identification of schreyerite and facilitate comparisons among occurrences from different geological settings. The relatively high TiO_2 content (58.20–59.05 wt.%) reported for the Rajasthan samples, compared with those from Russia (51–53 wt.%), further highlights the value of Raman spectroscopy when integrated with chemical and structural analyses for understanding compositional variations and the genesis of Ti-bearing refractory minerals (Parthasarathy et al., 2017).

Tungsten-Minerals

Occurrence of fluid deposited graphite along with accessory tungsten mineralization in the graphite schists/gneisses associated with graphitic garnetiferous sillimanite gneisses (khondalite group) of the Burugubanda-Tapaskonda shear zone. Fluid deposited rhombohedral graphite occurs as three lensoidal bodies varying from few centimeters to few meters in width and about 180-200 m in strike length and often reaching the depth of 80-100 m. Graphite schists/ gneisses are the host rocks for the tungsten mineralization. Tungsten minerals in the stream sediments and soils have been found in-situ ore deposits as heavy concentrates of tungsten in the vicinity of Burugubanda-Tapaskonda shear zone area. The amounts of 0.1-0.5 % WO_3 content bearing tungsten were identified along with fluid-deposited graphite from the shear zone area. Scheelite and ferberite are the most predominant accessory minerals which occur in the form of lustrous coarse crystalline, granular and disseminated varieties (Parthasarathy et al., 2006a). These geological and mineralogical characteristics make the Burugubanda–Tapasikonda Shear Zone an ideal natural setting for investigating hydrothermal carbon precipitation, graphite crystallization, and the genesis of graphite-associated tungsten mineralization.

Scheelite ($CaWO_4$) represents the dominant tungsten-bearing mineral reported from the Eastern Ghats Mobile Belt of India. Occurring chiefly within calc-silicate granulites, skarn-like assemblages, and quartz-rich metamorphic rocks, scheelite provides important evidence for tungsten mobilization during high-grade metamorphism and associated fluid activity (Biswal et al., 2000; Parthasarathy et al., 2006a, b). Raman spectroscopy provides a sensitive and non-destructive approach for the characterization of scheelite-type tungstates, enabling identification of WO_4 tetrahedral vibrations, evaluation of cation substitutions, assessment of structural disorder, and monitoring of pressure-induced phase transitions (Fig. 7). The characteristic room-temperature Raman bands are listed in Table 1. Among them, the most intense feature is the ν_1 symmetric stretching vibration of WO_4 tetrahedra near 911 cm^{-1}, which represents the principal Raman-active mode and serves as a diagnostic spectral fingerprint of scheelite-type tungstates.

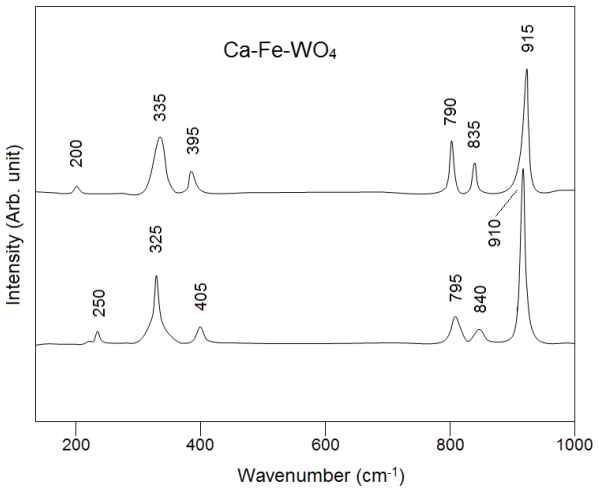


Fig. 7. Raman spectra of two Ca–Fe tungstate (Ca–Fe–WO_4) samples showing the characteristic vibrational modes of the scheelite-type structure.

Table 1. Characteristic room-temperature Raman bands and vibrational assignments of scheelite-type tungstates.

Raman Shift (cm^{-1})	Assignment
910-915	ν_1 symmetric W–O stretching (A_g)
790-840	ν_3 asymmetric stretching
395-405	ν_4 asymmetric bending
325-335	ν_2 symmetric bending
200-250	Rotational modes of WO_4 tetrahedral
80-150	External lattice modes

Geikielite

Geikielite ($MgTiO_3$), the magnesium-rich end member of the ilmenite group, is an important titanium-bearing mineral that serves as an indicator of Ti-enriched magmatic and high-grade metamorphic environments. Although it is rarely exploited as a primary titanium ore, geikielite is valuable for titanium resource assessment, heavy-mineral provenance studies, and exploration of associated critical mineral deposits (Haggerty, 1976; Parthasarathy et al., 2002). In India, geikielite occurs in the marble quarries near Rajapalayam, Southern Granulite Terrain, Tamil Nadu, where it is associated with forsterite,

Mg–Al spinel, titanoclinohumite, apatite, and carbonate minerals. This mineral assemblage records granulite-facies metamorphism and Ti-rich fluid activity related to the Pan-African tectono-metamorphic event (Parthasarathy, 2007a, b, 2011). Synthetic $MgTiO_3$ has also attracted considerable attention as a microwave dielectric ceramic because of its excellent dielectric properties and stability in electronic devices (Cogle et al., 1991; Parthasarathy, 2007a, b, 2011). Magnesium-based materials have emerged as promising candidates for next-generation rechargeable batteries owing to their high volumetric energy density, enhanced safety, superior cycling stability, and natural abundance, offering a sustainable alternative to lithium-based energy storage systems (Aurbach et al., 2001, 2007; Malachi et al., 2025; Li et al., 2026). The geikielite crystals investigated in this study contain minor ilmenite ($FeTiO_3$) as an impurity. Compositional analysis indicates an ilmenite content of approximately 0.3–0.4 wt.% $FeTiO_3$ (Janardhan et al., 2001; Chandra et al., 2010; Parthasarathy, 2011).

The vibrational characteristics of geikielite have been extensively investigated using Raman and FTIR spectroscopy. Geikielite crystallizes in an ilmenite-type structure (space group $R\bar{3}$), for which group-theoretical analysis predicts ten Raman-active phonon modes ($5Ag + 5Eg$). The Raman spectrum is characterized by intense bands at ~490 and ~720 cm^{-1}, representing the characteristic vibrational fingerprint of phase-pure geikielite and arising from TiO_6 octahedral vibrations. Additional Raman bands in the 200–620 cm^{-1} region are attributed to Ti–O stretching, bending, and lattice vibrational modes, providing a reliable basis for phase identification and compositional assessment within the ilmenite-group minerals (Parthasarathy, 2011). The FTIR spectrum exhibits prominent absorption bands at ~428, ~520, and ~680 cm^{-1}, corresponding to Ti–O stretching and Ti–O–Mg bending vibrations within the octahedral framework. Collectively, Raman and FTIR spectroscopy provide a rapid, non-destructive means of confirming phase purity, evaluating crystallinity, verifying stoichiometry, and detecting secondary phases such as $MgTi_2O_5$ and rutile TiO_2.

Cavansite

Vanadium-bearing minerals have attracted increasing attention owing to their geological significance, technological applications, and occurrence in terrestrial and extraterrestrial environments (Chaudhary et al., 2026). Among these, cavansite [$Ca(VO)Si_4O_{10}·4H_2O$] and schreyerite ($V_2Ti_3O_9$) represent two structurally distinct vanadium-bearing minerals that provide valuable insights into crystal chemistry, phase stability, and pressure-induced structural transformations. (Staples et al., 1973; Evans, 1973; Birch, 1977; Kothavala, 1991; Parthasarathy et al., 2008; Ravindran et al., 2012; Ottens et al., 2025; Chaudhary et al., 2026). Owing to its open-framework architecture, analogous to zeolites and other negative thermal expansion materials, cavansite provides an excellent model for investigating pressure-induced structural transformations and amorphization processes in hydrous silicates (Arora, 2000; Havenga et al., 2003; Ravindran et al., 2012). Raman and infrared spectroscopy have proven particularly valuable for probing its crystal chemistry, lattice dynamics, and the role of hydrous species during compression.

Factor-group analysis predicts 174 Raman-active and 133 infrared-active vibrational modes for cavansite; however, only about 36 Raman bands are experimentally observed under ambient conditions because of mode overlap, accidental degeneracy, and weak scattering intensities (Ravindran et al., 2012). The Raman spectrum is dominated by lattice vibrations below 300 cm^{-1}, Si–O stretching modes between 500 and 800 cm^{-1}, V=O stretching vibrations in the 900–1000 cm^{-1} region, and broad O–H stretching bands near 3546 cm^{-1} arising from crystallization water. The Raman spectrum of cavansite is dominated by an intense band at 981 cm^{-1} and pentagonite by a band at 971 cm^{-1} attributed to the stretching vibrations of $(SiO_3)n$ units. Cavansite is characterised by two intense bands at 574 and 672 cm^{-1} whereas pentagonite by a single band at 651 cm^{-1}.The intense blue colour is attributed to V^{4+} ions (Frost and Xi, 2012). These vibrational features provide important information on the framework structure and local bonding environment of the mineral (Ravindran et al., 2012).

High-pressure Raman studies reveal a sequence of pressure-induced structural modifications. Significant spectral changes occur near 1.1 GPa, including disappearance of selected lattice and internal modes, softening of the prominent V=O stretching vibration, and the appearance of new bands in the 2800–3400 cm^{-1} region associated with changes in hydrogen bonding (Ravindran et al., 2012). Additional mode splitting, frequency shifts, and emergence of new vibrational features at approximately 3, 4–5, 6, and 8 GPa indicate successive pressure-induced phase transitions (Fig. 8). Above ~14–15 GPa, sharp Raman bands collapse into a few broad features, signifying irreversible pressure-induced amorphization (Ravindran et al., 2012). The pronounced evolution of O–H-related vibrations demonstrates the important role of structurally bound water and hydrous species in governing the compression behavior of the mineral (Ringwood and Major, 1966; Ringwood, 1970; Arora, 2000; Ravindran et al., 2012)

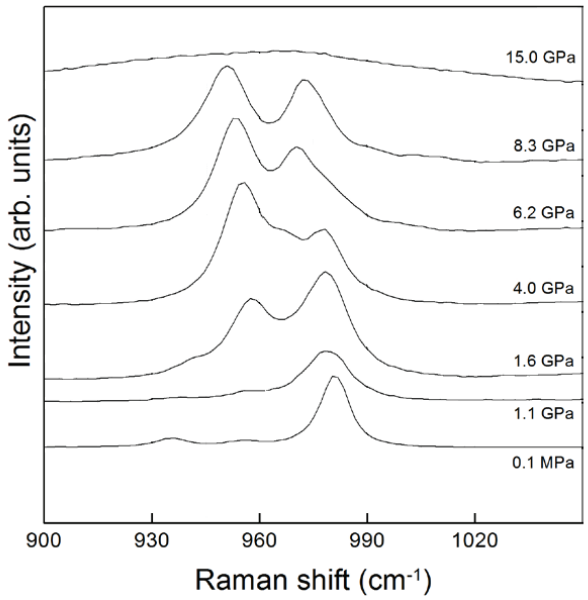


Fig. 8. Raman spectra of cavansite collected at different pressures, highlighting the pressure-induced evolution of the V=O stretching region (~935–950 cm^{-1}).

Infrared spectroscopy complements Raman observations by providing detailed information on O–H stretching vibrations and hydrogen-bonding interactions involving H_2O, OH^-, and H_3O^+ species. Subsequent structural studies have shown that cavansite contains H_3O^+ and OH^- in addition to H_2O, leading to a revised structural formula and highlighting the complexity of its hydrous framework (Evans, 1973; Ravindran et al., 2012). Variations in the O–H vibrational region suggest that these hydrous components may contribute significantly to the observed phase transitions and amorphization processes. Comparisons with other calcium silicates indicate that pressure-induced transformations to garnet-type, stishovite-bearing, and perovskite-type assemblages are common in Ca-bearing silicate systems (Ringwood, 1970; Ishida et al., 2009; Ravindran et al., 2012; Saikia et al., 2022a). Consequently, the combined application of Raman and infrared spectroscopy provides critical insights into framework stability, hydrogen-bonding evolution, phase transitions, and amorphization mechanisms in cavansite and related hydrous silicates under extreme conditions.

Cassiterite

Cobalt-doped cassiterite (Co-doped SnO_2) has attracted considerable attention because of its enhanced electrical conductivity, reduced optical bandgap, and defect-mediated surface reactivity compared with pristine SnO_2 (Acharya et al., 1982; Babu, 1994; Parthasarathy and Sreedhar, 2011). These characteristics make it a promising material for photocatalysis, gas sensing, lithium-ion battery anodes, and supercapacitors, where improved charge transport, ion diffusion, and electrochemical stability are essential. FTIR spectroscopy is an effective technique for probing the structural characteristics of Co-doped SnO_2, including metal–oxygen lattice vibrations, surface hydroxyl groups, adsorbed water molecules, and defect-related structural modifications (Fig. 9). The FTIR spectra are dominated by strong absorption bands in the 450–600 cm^{-1} region, which correspond to the Sn–O lattice vibrations of the tetragonal rutile-type cassiterite structure. Variations in the position, intensity, and width of these bands, together with changes in the hydroxyl and water-related vibrational features, provide valuable insights into Co incorporation, lattice distortion, oxygen-vacancy formation, and the local structural environment induced by cobalt substitution.

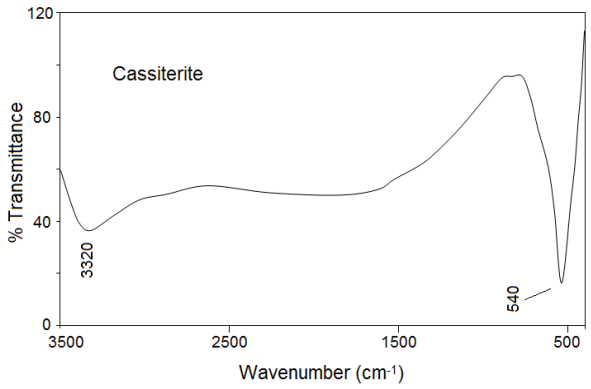


Fig. 9. FTIR spectrum of natural cassiterite (SnO_2) showing the characteristic Sn–O lattice vibration at ~540 cm^{-1} and a broad O–H stretching band centred at ~3320 cm^{-1}, attributed to surface-adsorbed water and hydroxyl groups.

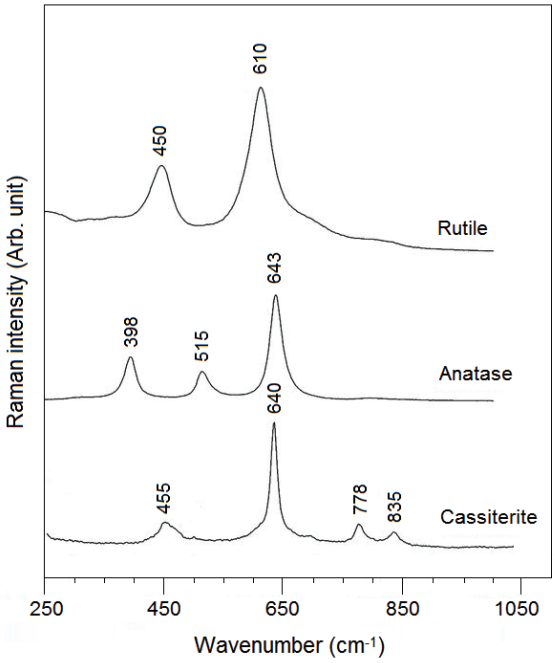


Fig. 10. Raman spectra of natural rutile (TiO_2), anatase (TiO_2), and cassiterite (SnO_2). Rutile exhibits characteristic Raman bands at ~450 and 610 cm^{-1}, whereas anatase is identified by its diagnostic modes at ~398, 515, and 643 cm^{-1}. Cassiterite displays the characteristic A1g mode at ~640 cm^{-1} together with weaker bands at ~455, 778, and 835 cm^{-1}, providing a distinctive spectral fingerprint for phase identification.

The Raman spectrum of cassiterite is dominated by the intense A1g mode at ~ 633 cm^{-1}, which serves as the principal diagnostic feature of the tetragonal rutile-type SnO_2 structure. The Eg (~475 cm^{-1}) and B2g (~775 cm^{-1}) modes further provide a characteristic spectral fingerprint for phase identification (Fig. 10). Variations in Raman peak position, bandwidth, and intensity, including the broadening and downshift of the A_{1g} mode, are commonly associated with lattice distortion induced by the substitution of trace elements such as Nb^{5+}, Ta^{5+}, and W^{6+}, These spectral variations also provide valuable insights into crystallinity, residual strain, pressure–temperature evolution, and trace-element incorporation, highlighting the utility of Raman spectroscopy in investigating cassiterite genesis, tin mineralization, and the evolution of ore-forming systems.

CONCLUSION

Vibrational spectroscopy, encompassing FTIR and Micro-Raman techniques, is a powerful, non-destructive analytical approach widely employed in the characterization of solid materials and minerals. Despite the growing strategic importance of critical minerals, relatively few studies have explored their characterization using vibrational spectroscopic methods. The present review seeks to highlight the relevance and potential of FTIR and Raman spectroscopy in the investigation of critical minerals and to demonstrate their

effectiveness in the rapid and reliable identification of mineral phases, elucidation of crystal structures and cation coordination environments, assessment of crystallinity, and detection of alteration products and secondary mineral phases.

The review demonstrate that Raman and FTIR spectroscopy provide detailed information on molecular bonding, lattice dynamics, structural disorder, and compositional variations while requiring minimal sample preparation and offering high spatial resolution and analytical sensitivity. Diagnostic Raman and FTIR bands serve as reliable fingerprints for identifying critical minerals, including cookeite (OH-stretching bands at ~3620–3700 cm^{-1} and Si–O vibrations at ~1000–1100 cm^{-1}), cavansite (V–O stretching at ~960–980 cm^{-1}), graphite (D and G bands at ~1350 and ~1580 cm^{-1}), cassiterite (A_{1g} mode at ~633 cm^{-1} with E_g and B_{2g} modes near ~475 and ~775 cm^{-1}), geikielite (Raman bands at ~490 and ~720 cm^{-1} together with FTIR bands at ~428, ~520, and ~680 cm^{-1}), scheelite (WO_4 symmetric stretching near ~910–915 cm^{-1}), and spodumene (Si–O stretching bands between ~700 and 1100 cm^{-1} with characteristic lattice modes below 600 cm^{-1}). These diagnostic spectral features provide rapid confirmation of mineral identity, crystallinity, structural disorder, chemical substitution, and phase purity, often without extensive sample preparation or destructive analyses.

In addition, vibrational spectroscopy can complement conventional analytical methods such as XRF and EPMA, particularly for minerals containing light elements such as lithium, where conventional techniques face inherent analytical limitations. However, Raman spectroscopy may be affected by fluorescence interference and laser-induced sample heating, whereas FTIR spectra can be complicated by overlapping absorption bands and generally provide limited quantitative compositional information. Consequently, vibrational spectroscopy is most effective when integrated with complementary mineralogical and geochemical techniques.

Owing to their versatility, sensitivity, and non-destructive nature, FTIR and Raman spectroscopy have become invaluable tools in mineral exploration, resource evaluation, and the investigation of ore-forming processes. Their ability to characterize minerals in situ and under varying pressure–temperature conditions further enhances their significance in critical mineral research, contributing to a deeper understanding of mineral genesis, crystallization processes, fluid–rock interactions, phase transformations, and the economic potential of strategic mineral resources. Continued advances in vibrational spectroscopy, combined with complementary mineralogical and geochemical techniques, will further improve the characterization, exploration, and sustainable utilization of critical mineral resources.

Acknowledgements: The authors are most grateful to Professor Tapas Kumar Biswal, IIT Bhubaneshwar, and the anonymous reviewers for their positive and constructive comments in improving the manuscript remarkably. We are grateful to Professor Sarada P. Mohanty and Dr. Ashit Kumar Swain Geological Survey of India for their kind invitation to submit this article to "Natural Resources and their utilization with special reference to Critical Minerals" (NATURE-CM 2026). We are grateful to Dr. Binoy Kr. Saikia, CSIR-North East Institute of Science and Technology, Jorhat, for his support and encouragement. GP is grateful to Department of Atomic Energy, Government of India for supporting under DAE-Raja Ramanna Chair Scheme.

References

Acharya, S., Sarangi, S.K. and Das, N.K. (1982) The Tin Ore Deposit of Orissa, India, in Amstutz, G.C., et al., (ed.) Ore Genesis. Special Publication of the Society for Geology Applied to Mineral Deposits, Springer, Berlin, Heidelberg, v.2. https://doi.org/10.1007/978-3-642-68344-2_30

Alshameri, A., He, H., Xin, C., Zhu, J., Xinghu, W., Zhu, R., and Wang, H. (2019) Understanding the role of natural clay minerals as effective adsorbents and alternative source of rare earth elements: Adsorption operative parameters. Hydrometallurgy**,** v.185**,** pp.149–161. http://dx.doi.org/10.5772/intechopen.87260

Anderson, A.J. and Maccarron, T. (2011) Three-dimensional textural and chemical characterization of polyphase inclusions in spodumene using a dual focused ion beam–scanning electron microscope (FIB–SEM). Can. Mineral.**,** v.49**,** pp.541–553. https://doi.org/10.3749/canmin.49.2.541

Anderson, A.J., Clark, A.H. and Gray, S. (2001) The occurrence and origin of zabuyelite (Li_2CO_3) in spodumene-hosted fluid inclusions: Implications for the internal evolution of rare-element granitic pegmatites. Can. Mineral.**,** v.39**,** pp.1513–1527. https://doi.org/10.2113/gscanmin.39.6.1513

Anderson, A.J. (2013) Are silicate-rich inclusions in spodumene crystallized aliquots of boundary layer melt? Geofluids**,** v.13**,** pp.460–466. https://doi.org/10.1111/gfl.12041

Arora, A.K. (2000) Pressure-induced amorphization versus decomposition. Solid State Commun., v.115**,** pp.665–668. https://doi.org/10.1016/S0038-1098(00)00253-2

Aurbach, D., Gofer, Y., Lu, Z., Schechter, A., Chusid, O., Gizbar, H., Cohen, Y., Ashkenazi, V., Moshkovich, M., Turgeman, R. and Levi, E. (2001) A short review on the comparison between Li battery systems and rechargeable magnesium battery technology. J. Power Sources, v.97–98, pp.28–32. https://doi.org/10.1016/S0378-7753(01)00585-7

Aurbach, D., Markovsky, B., Salitra, G., Markevich, E., Talyossef, Y., Koltypin, M., Nazar, L., Ellis, B. and Kovacheva, D. (2007) Review on electrode–electrolyte solution interactions, related to cathode materials for Li-ion batteries. *J. Power Sources,* v.165, pp.491–499. https://doi.org/10.1016/j.jpowsour.2006.10.025

Babu, T.M. (1994) Tin in India. Geological Society of India, Bangalore, pp.217.

Beyssac, O., Rouzaud, J.N., Goffé, B., Brunet, F. and Chopin, C. (2002) Graphitization in a high-pressure, low-temperature metamorphic gradient: A Raman microspectroscopy and HRTEM study. Contrib. Mineral. Petrol.**,** v.143**,** pp.19–31. https://doi.org/10.1007/s00410-001-0324-7

Birch, W. (1977) Cavansite from the Poonah district, India. Mineral. Rec.,v.8, pp.61.

Biswal, T.K., Jena, S.K., Datta, S., Das, R. and Khan, K. (2000) Deformation of terrane boundary shear zone (Lakhna shear zone) between Eastern Ghats Mobile Belt and Bastar craton in Balangir and Kalahandi districts, Orissa. *J. Geol. Soc. India,* v. 55 (4), pp.367-380. https://doi.org/10.17491/jgsi/2000/550402

Bobos, I., Vieillard, P., Charoy, B. and Noronha, F. (2007) Alteration of spodumene to cookeite and its pressure and temperature stability conditions in Li-bearing aplite–pegmatites from northern Portugal. Clays Clay Miner.**,** v.55, pp.295–310. https://doi.org/10.1346/CCMN.2007.0550306

Bradbury, M.H. and Baeyens, B. (2002) Sorption of Eu on Na- and Ca-montmorillonites: Experimental investigations and modelling

with cation exchange and surface complexation. Geochim. Cosmochim. Acta, v.66, pp.2325–2334. https://doi.org/10.1016/S0016-7037(02)00841-4

Chandra, U., Sharma, P., Parthasarathy, G., and Sreedhar, B. (2010) ^{57}Fe Mössbauer spectroscopy and electrical resistivity studies on naturally occurring native iron under high pressures up to 9.1 GPa. Am. Mineral., v.95, pp.870–875.

Chaudhary, P.L., Bora, M.A., Rambabu, U. Rajurkar, N.S. and Adhyapak, P.V. (2026) Identification and Characterization of Cavansite with Its Associated Minerals Acquired from Wagholi Quarry, Pune (Maharashtra), India. JOM, v.78, pp.5882–5890. https://doi.org/10.1007/s11837-026-08193-w

Cogle, T.J., Mateus, C.A.S., Binks, J.H. and Irvine, J.T.S. (1991) Solid-solution formation, electrical properties and zero-resistance behaviour in the spinel system Mg_2TiO_4–$MgTi_2O_4$. J. Mater. Chem., v.1, pp.289–291. https://doi.org/10.1039/JM9910100289

Coppin, F., Berger, G., Bauer, A., Castet, S. and Loubet, M. (2002) Sorption of lanthanides on smectite and kaolinite. Chem. Geol., v.182, pp.57–68.

Courrèges-Lacoste, B. G., Ahlers, B. and Rull Pérez, F. (2007) Combined Raman spectrometer/laser-induced breakdown spectrometer for the next ESA mission to Mars. *Spectrochim. Acta A Mol. Biomol. Spectrosc.,* v.68, pp.1023–1028. https://doi.org/10.1016/j.saa.2007.03.026

Ding, X., Li, J., Chou, I.-M., Chen, Z. and Li, S. (2020) Raman spectroscopic identification of cookeite in the crystal-rich inclusions in spodumene from the Jiajika lithium pegmatite deposit, China, and its geological implications. *Eur. J. Mineral.,* v.32, pp.67–75. https://doi.org/10.5194/ejm-32-67-2020

Dissanayake, C.B. (1981) The origin of graphite of Sri Lanka. Org. Geochem., v.3, pp.1–7. https://doi.org/10.1016/0146-6380(81)90006-1

Dobelin, N., Reznitsky, L.Z., Sklyarov, E. and Armbruster, T. (2006) Schreyerite $V_2Ti_3O_9$: New occurrence and crystal structure. *Am. Mineral.,* v.91, pp.196–202. https://doi.org/10.2138/am.2006.1893

Evans, H.T. (1973) The crystal structures of cavansite and pentagonite. Am. Mineral., v.58, pp.412–424.

Farmer, V.C. (1974) *The Infrared Spectra of Minerals*. Mineralogical Society, London.

Frost, R.L. and Rintoul, L. (1996) Lattice vibrations of montmorillonite: An FT Raman and X-ray diffraction study. Appl. Clay Sci., v.11, pp.171–183. https://doi.org/10.1016/S0169-1317(96)00017-8

Frost, R.L. (1995) Fourier transform Raman spectroscopy of kaolinite, dickite and halloysite. Clays Clay Miner., v.43, pp.191–195.

Frost, R.L. and Xi, Y. (2012) Vibrational spectroscopic study of the minerals cavansite and pentagonite $Ca(V^{4+}O)Si_4O_{10}{\cdot}4H_2O$. Spectrochim. Acta A, v.95, pp.263-269. https://doi.org/10.1016/j.saa.2012.04.021

Haggerty, S.E. (1976) Opaque mineral oxides in terrestrial igneous rocks. In: Rumble, D., III (Ed.), *Oxide Minerals*. Rev. Mineral., v.3, pp.101–176.

Harmon, R.S. (2024) Laser-Induced Breakdown Spectroscopy in Mineral Exploration and Ore Processing. *Minerals,* v.14, pp.731. https://doi.org/10.3390/min14070731

Havenga, E.A., Huang, Y. and Secco, R.A. (2003) An investigation of the effect of high pressure on the structure of siliceous zeolite Y. Mater. Res. Bull., v.38, pp.381–391. https://doi.org/10.1016/S0025-5408(02)01061-9

Haxel, G.B., Hedrick, J.B. and Orris, G.J. (2002) *Rare Earth Elements—Critical Resources for High Technology.* U.S. Geological Survey

Henry, D.G., Jarvis, I., Gillmore, G. and Stephenson, M. (2019) Raman spectroscopy as a tool to determine the thermal maturity of organic matter: Application to sedimentary, metamorphic and structural geology. Earth Sci. Rev., v.198, pp.102936. https://doi.org/10.1016/j.earscirev.2019.102936

Hoeller, W. and Stumpfi, E.F. (1995) Cr–V oxides from Rampura-Agucha Pb–Zn–(Ag) deposit, Rajasthan, India. *Can. Mineral.,* v.33, pp.745–752.

Ishida, N., Kimata, M., Nishida, N., Hatta, T., Shimizu, M. and Akasaka, T. (2009) Crystal chemistry and structural refinement of cavansite. J. Mineral. Petrol. Sci., v.104, pp.241–252.

Janardhan, A.S., Sriramguru, Basava, S., and Shankara, M.A. (2001) Geikilite-Mg.Al.Spinel-Titanoclinohumite association from a Marble Quarry near Rajapal-aiyam Area, Part of 500 Ma Old Southern Granulite Terrain, Southern India. Gondwana Res., v.4, pp.359–366.

Jehlička, J. and Edwards, H.G.M. (2008) Raman spectroscopy as a tool for the non-destructive identification of organic minerals in the geological record. Org. Geochem., v.39, pp.371–386. https://doi.org/10.1016/j.orggeochem.2008.01.005

Kelemen, S.R. and Fang, H.L. (2001) Maturity trends in Raman spectra from kerogen and coal. Energy Fuels, v.15, pp.653–658. https://doi.org/10.1021/ef0002039

Kothavala, R.Z. (1991) The Wagholi cavansite locality near Poona, India. Mineral. Rec.,v.22, pp.415–420.

Kumar, A. and Lingfa, P. (2020) Sodium bentonite and kaolin clays: Comparative study on their FT-IR, XRF, and XRD. Mater. Today Proc., v.22, pp.737–742. https://doi.org/10.1016/j.matpr.2019.10.037

Li, J. and Chou, I.M. (2016) An occurrence of metastable cristobalite in spodumene-hosted crystal-rich inclusions from the Jiajika pegmatite deposit, China. J. Geochem. Explor., v.171, pp.29–36. https://doi.org/10.1016/j.gexplo.2015.10.012

Li, J., Diao, J., Tao, H., Qin, H., Wang, Z., Zhou, H. and Li, H.Y. (2026) Synthesis and electrochemical study of $MgTi_2O_5$: A pseudo-brookite cathode for rechargeable magnesium batteries. *Nanoscale.* http://dx.doi.org/10.1039/D6NR00905K

Luque, F.J., Pasteris, J.D., Wopenka, B., Rodas, M. and Barrenechea, J.F. (1998) Natural fluid-deposited graphite: Mineralogical characteristics and mechanisms of formation. *Am. J. Sci.,* v.298, pp.471–498. https://hdl.handle.net/20.500.14352/57786

Madejová, J. and Komadel, P. (2001) Baseline studies of the Clay Minerals Society source clays: Infrared methods. *Clays Clay Miner.,* v.49, pp.410–432.

Malachi, I.O., Olawumi, A.O., Afolabi, S.O. and Oladapo, B.I. (2025) Looking Beyond Lithium for Breakthroughs in Magnesium-Ion Batteries as Sustainable Solutions. *Sustainability,* v.17, pp.3782. https://doi.org/10.3390/su17093782

Moldoveanu, G.A. and Papangelakis, V.G. (2012) Recovery of rare earth elements adsorbed on clay minerals: I. Desorption mechanism. *Hydrometallurgy,* v.117–118, pp.71–78. https://doi.org/10.1016/j.hydromet.2012.02.007

Moldoveanu, G.A. and Papangelakis, V.G. (2013) Recovery of rare earth elements adsorbed on clay minerals: II. Leaching with ammonium sulfate. *Hydrometallurgy,* v.131–132, pp.158–166.

https://doi.org/10.1016/j.hydromet.2012.10.011

Moroz, T.N., Edwards, H.G.M. and Zhmodik, S.M. (2021) Detection of carbonate, phosphate minerals and cyanobacteria in rock from the Tomtor deposit, Russia, by Raman spectroscopy. *Spectrochim. Acta A Mol. Biomol. Spectrosc.,* v.250, pp.119372. https://doi.org/10.1016/j.saa.2020.119372

Nayak, P.S. and Singh, B.K. (2007) Instrumental characterization of clay by XRF, XRD and FTIR. *Bull. Mater. Sci.* v.30, pp.235–238. https://doi.org/10.1007/s12034-007-0042-5

Ottens, B., Duraiswami, R.A. and Krenn, K. (2025) The formation of Cavansite and Pentagonite in the Wagholi Quarries, Pune, India. Minerals, v.15, pp.126. https://doi.org/10.3390/min15020126

Pani, S., Singh, S.K. and Mohapatra, B.K. (2016) Vibrational Spectroscopic Study for Qualitative Assessment of Mn-oxide Ore. Resour. Geol., v.66(1), pp.12–23. https://doi.org/10.1111/rge.12083

Parthasarathy, G. (2007a) Electrical resistivity of nano-crystalline and natural $MgTiO_3$-geikielite at high pressures up to 8 GPa. *Mater. Lett.,* v.61, pp.4329–4331. https://doi.org/10.1016/j.matlet.2007.01.097

Parthasarathy, G. (2007b) High-temperature electrical resistivity and heat capacity studies on nano-crystalline geikielite. *Mater. Lett.,* v.61, pp.3208–3210. https://doi.org/10.1016/j.matlet.2006.11.028

Parthasarathy, G. (2011) Electrical properties of natural and synthetic nano-crystalline $MgTiO_3$ geikielite at mantle pressure and temperature conditions. *Am. Mineral.,* v.96, pp.860–863. https://doi.org/10.2138/am.2011.3660

Parthasarathy, G. and Sreedhar, B. (2011) Pressure dependence of the electrical resistivity of natural cassiterite SnO_2 and of undoped and Co-doped nanocrystalline SnO_2 . Philosophical Magazine Letters, v.91(3), pp.200–206. https://doi.org/10.1080/09500839.2010.547226

Parthasarathy, G. and Sharma, S.R. (2001) A comparative study on structural properties of graphites from Dharwar Craton, India: A high-temperature DTA study. *J. Geol. Soc. India*, v.57, pp.435–442.

Parthasarathy, G., Sharma, S.R. and Hussain, S.M. (2002) High-temperature studies on graphite from East Antarctica. *J. Appl. Geochem.,* v.4, pp.263–270.

Parthasarathy, G., Sharma, S.R., Ravindran, T.R., Arora, A.K. and Hussain, S.M. (2003) Structural and thermal studies of graphite from East Antarctica. *J. Geol. Soc. India,* v.61, pp.335–343.

Parthasarathy, G., Collins, A. S. and Chetty, T. R. K. (2006a) Natural Graphite from Neoproterozoic Psammitic Gneiss, Inanalo Mountain, Southern Madagascar. *J. Geol. Soc. India, v.* 68(2), pp.176–180. https://doi.org/10.17491/jgsi/2006/680202

Parthasarathy, G., Sreedhar, B. and Chetty, T.R.K. (2006b) Spectroscopic and X-ray diffraction studies on fluid deposited rhombohedral graphite from the Eastern Ghats Mobile Belt, India. *Curr. Sci.,* v.90(7), pp.995–1000.

Parthasarathy, G. Mookherjee, A. and Kunwar, A. (2008) Pressure-induced phase transition in cavansite—A rare zeolite from the Deccan Trap, India. Geochim. Cosmochim. Acta, v.73, pp.999.

Parthasarathy, G., Chandra, U. and Saikia, B.J. (2017) Powder XRD, thermal and spectroscopic characterization of schreyerite $V_2Ti_3O_9$, a rare vanadium–titanium oxide mineral from the Pb–Zn ore deposit, Bhilwara, Rajasthan, India, *Goldschmidt Conf. Abstr.*

Peng, Z., Chang, X., Zhang, G., Shi, B., Guo, R., Zhang, J., Wang, C., Wang, S., Li, Y. and Li, Z. (2026) Application of Raman-infrared spectroscopy in the evaluation of organic matter characteristics and thermal maturity of highly- to overmature source rocks. *Unconventional Resour.,* v.12, pp.100364. https://doi.org/10.1016/j.uncres.2026.100364

Pommier, C.J.S., Denton, B. and Downs, R.T. (2003) Raman spectroscopic study of spodumene ($LiAlSi_2O_6$) through the pressure-induced phase change from C2/c to $P2_1/c$. *J. Raman Spectrosc.,* v.34, pp.769–775. https://doi.org/10.1002/jrs.1051

Ramakrishnan, M., Nanda, J.K. and Augustine, P.F. (1998) Geological evolution of the Proterozoic Eastern Ghats Mobile Belt. *Geol. Surv. India Spec. Publ.,* v.44, pp.1–21.

Ravindran, T.R., Arora, A.K. and Parthasarathy, G. (2012) Raman spectroscopic study of pressure induced amorphization in cavansite. *J. Phys. Conf. Ser.,* v.377, pp.012004. https://doi.org/10.1088/1742-6596/377/1/012004

Ringwood, A.E. and Major, A. (1966) High-pressure transformations in pyroxenes. *Earth Planet. Sci. Lett.,* v.1, pp.351–357.

Ringwood, A.E. (1970) Phase transformations and the constitution of the mantle. *Phys. Earth Planet. Inter.,* v.3, pp.109–155.

Ritz, M., Vaculíková, L., Plevová, E., Matýsek, D. and Mališ, J. (2012) Determination of the predominant minerals in sedimentary rocks by chemometric analysis of infrared spectra. *Clays Clay Miner.,* v.60, pp.655–665.

Rull-Pérez, F. and Martinez-Frias, J. (2006) Raman spectroscopy goes to Mars. *Spectrosc. Eur.,* v.18, pp.18–21.

Saikia, B.J., Parthasarathy, G. and Sarmah, N.C. (2008) Fourier transform infrared spectroscopic estimation of crystallinity in SiO_2 based rocks. *Bull. Mater. Sci.,* v.31, pp.775–779.

Saikia, B.J., Parthasarathy, G. and Sarmah, N.C. (2009) Fourier transform infrared spectroscopic characterization of Dergaon H5 chondrite: Evidence of aliphatic organic compound. *Nature Sci.,* v.7, pp.45–51.

Saikia, B.J. and Parthasarathy, G. (2010) Fourier Transform Infrared Spectroscopic Characterization of Kaolinite from Assam and Meghalaya, Northeastern India. *J. Mod. Phys.,* v.1, pp.206–210. https://doi.org/10.4236/jmp.2010.14031

Saikia, B.J., Parthasarathy, G., Borah, R.R. and Borthakur, R. (2016) Raman and FTIR spectroscopic evaluation of clay minerals and estimation of metal contaminations in natural deposition of surface sediments from Brahmaputra River. *Int. J. Geosci.*, v.7, pp.873–883. http://dx.doi.org/10.4236/ijg.2016.77064

Saikia, B.J., Parthasarathy, G. and Borah, R.R. (2017) Nanodiamonds and silicate minerals in ordinary chondrites as determined by micro-Raman spectroscopy. *Meteorit. Planet. Sci.,* v.52, pp.1146–1154. https://doi.org/10.1111/maps.12850

Saikia, B.J., Parthasarathy, G. and Borah, R.R. (2018) Raman and infrared spectroscopic tentative identification of organic traces in Sadiya (LL5) ordinary chondrite. *Adv. Astrophys.,* v.3, pp.250–256. https://doi.org/10.22606/adap.2018.34004

Saikia, B.J., Parthasarathy, G., Gorbatsevich, F.F. and Borah, R.R. (2021) Characterization of amphiboles from the Kola super-deep borehole, Russia by Raman and infrared spectroscopy. *Geosci. Front.,* v.12, pp.101134. https://dx.doi.org/10.1016/j.gsf.2020.12.013

Saikia, B.J., Parthasarathy, G. and Borah, R.R. (2022a) High-pressure polymorphs of olivine and silica in Kamargaon (L6) chondrite by laser micro-Raman and XRD studies. *J. Earth Syst. Sci.,* v.131,

pp.38. https://doi.org/10.1007/s12040-021-01803-y

Saikia, B.J., Parthasarathy, G., Chalapathi Rao, N.V., Borah, R.R. and Kumar, D. (2022b) High shock pressure metamorphism induced transformations of olivine and feldspar in Natun Balijan L4 chondrite: Evidence from micro-Raman, infrared spectroscopy, X-ray diffraction and electron microprobe analysis. *J. Geol. Soc. India,* v.98, pp.731–739. https://doi.org/10.1007/s12594-022-2061-7

Saikia, B.J., Basak, S., Borah, R.R. and Parthasarathy, G. (2022c) Spectroscopic investigations and mineral chemistry of dunite from the Sargur Supracrustals (3 Ga) Greenstone Belt: Implications to terrestrial analogues for lunar and Martian dunite. *J. Geol. Soc. India,* v.98, pp.1505–1512. https://doi.org/10.1007/s12594-022-2205-9

Saikia, B.J., Parthasarathy, G. and Borah, R.R. (2022d) Investigations of organic matter in meteorites using Fourier transform infrared and micro-Raman spectroscopic methods: Implications for origin of extraterrestrial organic matter. *J. Ind. Geophys. Union,* v.26, pp.62–77.

Saikia, B.J., Parthasarathy, G., Saikia, B.K. and Borah, R.R. (2023) Occurrence of natural fullerene C_{60} from the iridium-rich Cretaceous–Paleogene (K–Pg) boundary layers of the Um-Sohryngkew River section, Meghalaya, India. *Carbon Trends*, v.13, pp.100309. https://doi.org/10.1016/j.cartre.2023.100309

Saikia, B.J., Parthasarathy, G., Chalapathi Rao, N.V., Seth, V. and Borah, R.R. (2024) Mineral chemistry of Mahadevpur H4/5 chondrite: Characterization of nanodiamonds through micro-Raman spectroscopic studies. *Curr. Sci.,* v.126, pp.574–582. https://doi.org/10.18520/cs/v126/i5/574-582

Saikia, B.J., Parthasarathy, G., Saikia, B.K., Bordoloi, P., Borah, R.R., Srivastava, P.K. and Satyanarayanan, M. (2026) Nanocrystalline Cookeite from Lithium Mineral Deposits of Jammu, India: A Multianalytical Characterization. *Earth Syst. Resour. Sustain.,* v.1**,** pp.97–109. https://doi.org/10.53941/esrs.2026.100006

Sarkar, S., Santosh, M., Dasgupta, S. and Fukuoka, M. (2003) Very high density CO_2 associated with ultrahigh-temperature metamorphism in the Eastern Ghats granulite belt, India. *Geology,* v.31, pp.51–54. https://doi.org/10.1130/0091-7613(2003)031%3C0051:VHDCAW%3E2.0.CO;2

Schito, A., Romano, C., Corrado, S., Grigo, D. and Poe, B. (2017) Diagenetic thermal evolution of organic matter by Raman spectroscopy. *Org. Geochem.,* v.106, pp.57–67. https://doi.org/10.1016/j.orggeochem.2016.12.006

Sharma, S.R., Parthasarathy, G., Ravindran, T.R., Arora, A.K. and Kumar, B. (2000) Laser Raman spectroscopic studies on graphites from Dharwar Craton: A possible metamorphic grade indicator for the host rocks. *J. Geol. Soc. India,* v.55, pp.413–420.

Sharma, S.R., Parthasarathy, G., Ravindran, T.R., Arora, A.K. and Hussain, S.M. (2001) Laser Raman spectroscopic studies on graphite from East Antarctica. *Polar Geosci.,* v.14, pp.159–167.

Staples, L.W., Evans, H.T. Jr. and Lindsay, J.R. (1973) Cavansite and pentagonite, new dimorphous calcium vanadium silicate minerals from Oregon. *Am. Mineral.,* v.58, pp.405–412.

Umathay, R.M. and Pophare, A.M. (2014) Revisit to Graphite-Tungsten Deposits of East Godavari District, Andhra Pradesh. J. Geol. Soc. India, v. 84 (4), pp.417–430. https://doi.org/10.1007/s12594-014-0147-6

Wang, R., Ramanaidou, E., Kirkland, C.L., Pejcic, B., Laukamp, C., Verrall, M., Schoneveld, L.E., Owen, N., Huang, S., Bath, A., Zhao, L. and Wang, Q. (2025) Genesis of cookeite, the primary lithium mineral in the Late Carboniferous strata of the North China Craton. *Ore Geol. Rev.,* v.186, pp.106903. https://doi.org/10.1016/j.oregeorev.2025.106903

Wopenka, B. and Pasteris, J.D. (1993) Structural characterization of kerogens to granulite-facies graphite: Applicability of Raman microprobe spectroscopy. *Am. Mineral.,* v.78, pp.533–557.

Xiao, Y.F., Huang, L., Long, Z.Q., Feng, Z.Y. and Wang, L.S. (2016) Adsorption ability of rare earth elements on clay minerals and its practical performance. *J. Rare Earths* v.34, pp.543–548. https://doi.org/10.1016/S1002-0721(16)60060-1

Xu, F., Onel, O., Council-Troche, M., Noble, A., Yoon, R.-H. and Morris, J.R. (2021) A study of rare earth ion-adsorption clays: The speciation of rare earth elements on kaolinite at basic pH. Appl. Clay Sci.**,** v.201**,** pp.105920. https://doi.org/10.1016/j.clay.2020.105920

Zhang, S., Liu, Q., Gao, F., Li, X., Liu, C., Li, H., Boyd, S.A., Johnston, C.T. and Teppen, B.J. (2017) Mechanism associated with kaolinite intercalation with urea: Combination of infrared spectroscopy and molecular dynamics simulation studies. *J. Phys. Chem. C,* v.121, pp.402–409. https://doi.org/10.1021/acs.jpcc.6b10533

Zhang, J., Zhao, B. and Schreiner, B. (2016) Rare Earth Beneficiation and Hydrometallurgical Processing. In: *Separation Hydrometallurgy of Rare Earth Elements. Springer International Publishing*, Cham, Switzerland, pp.19–54.

Zhou, H. and Zihyun, L.T. (2025) Analyzing the supply-demand dynamics of critical minerals for clean energy technologies: Impact of per value-added energy intensity. *Energy,* v.335, pp.137816. https://doi.org/10.1016/j.energy.2025.137816